Smart Metering of Variable Power Loads

Warit Wichakool, *Member, IEEE,* Zachary Remscrim, Uzoma A. Orji, *Student Member, IEEE,*
and Steven B. Leeb, *Fellow, IEEE*

Abstract—Nonintrusive load monitoring (NILM) seeks to determine the operation of individual loads in a building strictly from measurements made on an aggregate current signal serving a collection of loads. Great strides have been made in performing NILM for loads whose operating state can be represented by a finite-state machine, i.e., loads that consume discrete or distinct power levels for periods of time. It is much more difficult to track the operation of continuously variable loads that demand ever-changing power. These loads are becoming more prevalent as variable speed drives, daylight-responsive lighting, and other power electronic controlled loads emerge on the grid. This paper demonstrates a method for tracking the power consumption of variable demand loads nonintrusively. The method applies to any site where NILM might be of interest, including commercial and industrial buildings, residences, and transportation systems.

Index Terms—Cyclotomic field, nonintrusive load monitoring (NILM), variable power load estimation, waveform-based modeling.

I. INTRODUCTION

BOTH UTILITIES and consumers will likely find innumerable ways to mine information if made available in a useful form. However, appropriate sensing and information delivery systems remain a chief bottleneck for many applications, and metering hardware and access to metered information will likely limit the implementation of new electric energy conservation strategies in the near future. The U.S. Department of Energy has identified "sensing and measurement" as one of the "five fundamental technologies" essential for driving the creation of a "smart grid" [4]. Consumers will need "simple, accessible, ..., rich, and useful information" to help manage their electrical consumption without interference in their lives [4].

Smart grid and smart meter initiatives seek to enable energy providers and consumers to intelligently manage their energy needs through real-time monitoring, analysis, and control. Power electronics and power electronic controls are proliferating in consumer electronics. There is an increasing expectation that advanced power conditioning electronics will play a role in managing and coordinating power consumption not simply for a particular load (such as a variable speed drive in an

air conditioning plant) but also in response to the dynamic needs and capability of the utility system. Loads that can respond not only to their own tasking but also to the needs of the utility are implicit in many visions of a smart grid. Monitoring the behavior of these loads with cost-effective nonintrusive monitoring techniques is a challenge because these loads can continuously vary their power consumption, blinding a meter from the distinct power changes typically used to track energy consumption using a nonintrusive load monitor (NILM) [5], [6].

A NILM system is a "smart" metering device designed to disaggregate the power consumption of each load from aggregate electrical measurements. Each load is identified by real and reactive power consumption and its current harmonics during a start-up transient or steady-state operation [3], [6]–[9]. The pattern recognition algorithm used in the NILM exploits the fact that many loads such as lights and motors consume approximately discrete power levels. A NILM with a transient event detector can recognize turn-on and turn-off events and track energy consumption. Great strides have been made in performing NILM for loads whose operating state can be represented by a finite-state machine, i.e., loads that consume discrete or distinct power levels for periods of time. This approach has become widely applied, and a wide variety of estimation techniques including transversal filters, clustering algorithms, multilevel wavelet transforms, artifical neural networks, and fuzzy estimators have been used to recognize and track power changes for nonintrusive monitoring [2], [10]–[14].

It is much more difficult to track the operation of continuously variable loads that demand ever-changing power. This fact is typically ignored. For example, Dong *et al.* [14] noted that "this limitation is fair because in actual operation these devices are expected to operate in a specific mode for large proportions of their operating time." Variable loads are often relegated as "unidentifiable" or ignored during nonintrusive monitoring, with energy estimates corrected post facto using other checks or logic, like a power consumption tally that adjusts results. Unfortunately, methods that ignore variable loads limit real-time disaggregation and monitoring, especially important for smart grid control and diagnostics application. Continuously variable loads are becoming more prevalent, as variable speed drives (VSDs), daylight-responsive lighting, and other power electronic controlled loads emerge on the grid.

This paper demonstrates a method for tracking the power consumption of variable demand loads nonintrusively. Experimental results will demonstrate that the total variable power load can be separated or disaggregated from loads with fixed steady-state consumption. A wide variety of estimators

could be used with the proposed method. The goal of this paper is to expose mathematics and physics-based modeling of loads to permit and enable real-time tracking of the total consumption of loads with continuously variable power demand. This paper introduces a new method for estimating the real and reactive power consumed by a continuously variable load such as a VSD operating in a collection of electrical loads. This method estimates the power consumption of the variable load given only aggregate measurements of current. The algorithm exploits structural features of the nonsinusoidal current waveform consumed by many variable power loads. The proposed method is distinct in requiring no internal circuit model or description of the variable load.

The application of power electronics enables many loads to operate over a wide variable power range. Examples of variable power loads are VSDs, computers, and light dimmers. These continuously variable power loads do not have a unique power consumption pattern. Therefore, these loads cannot necessarily be tracked for energy consumption strictly by examining turn-on and turn-off transients. Loads like VSDs may consume harmonic currents such as the fifth and seventh harmonics. At a particular site, these harmonics may be uniquely associated with the VSD and can be used to estimate the fundamental current harmonic and the power consumption of the VSD accurately using a data-driven model [1]. The estimating function based on empirical data is sensitive to changes in the environment such as input voltage harmonics [15]. An alternative estimator was developed by modeling and analyzing the behavior of the internal circuit of the VSD, specifically the uncontrolled three-phase rectifier [15]. The model-based estimator solves the issue of the input voltage distortions, enhancing the robustness of the estimator. However, other loads may be too complex to model and analyze. Therefore, the application of the model-based estimator for other variable power loads may not be possible.

Although these variable power loads consume different harmonic currents, there are common characteristics in the current among these loads. These variable power loads are not linear time invariant because their currents are modulated by operations of power electronics. As a result, their currents are nonsinusoidal. However, the current waveforms of these variable power loads consist of structural features that can be identified in both the time and frequency domains. For example, the current waveforms of VSDs and computers have known regions of zero current. Furthermore, the sampled current signal is also band-limited and periodic. These observable characteristics of the current waveforms can be used to write linear constraints according to the Fourier analysis and synthesis equations. These constraints can be manipulated using a standard Gaussian elimination method to achieve a functional relationship between the fundamental current harmonic and higher harmonics uniquely associated with the load. The estimator can be computed without fully analyzing the underlying circuit of the load. In addition, the actual computation can be done using a cyclotomic field representation to minimize numerical error [16]–[19].

This paper describes a systematic process to derive a waveform-based estimator. The first section describes the
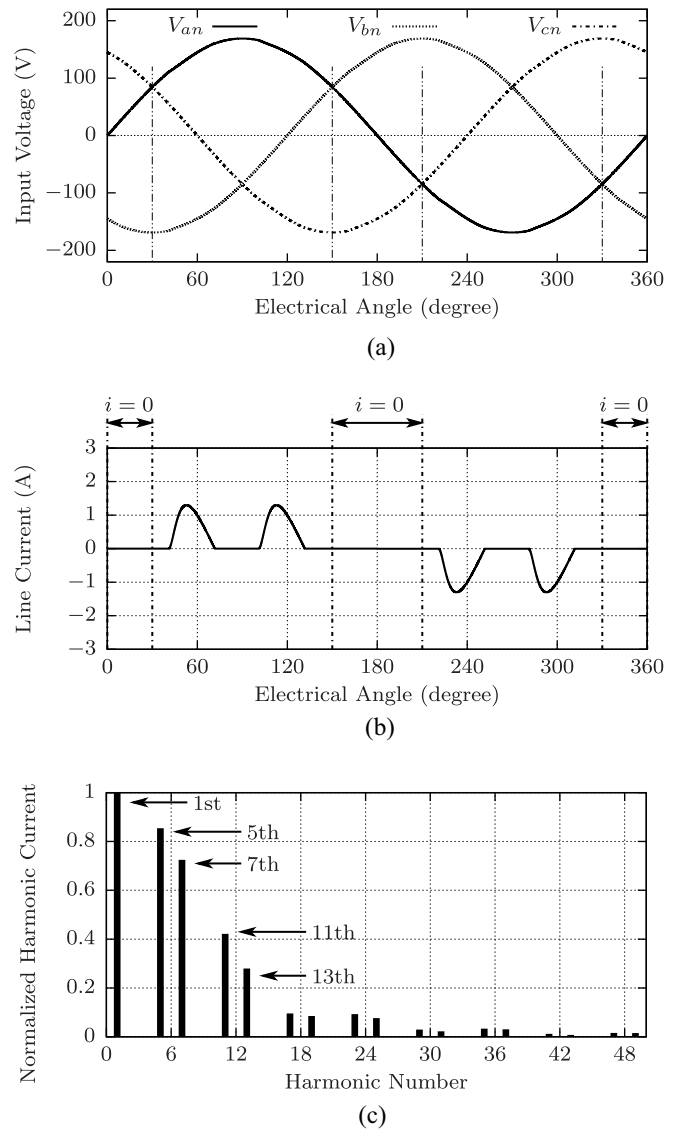

Fig. 1.   Simulated voltage and current waveforms and current harmonics associated with a VSD. (a) Three-phase voltages. (b) VSD line current for one cycle. (c) Normalized harmonic currents.

waveform features and their connections to the Fourier analysis and synthesis equations. The next section explains a four-step process to compute the estimator for a particular load. Finally, the paper includes experimental results demonstrating the capability of the waveform-based estimator to disaggregate the power consumption of continuously variable power loads such as VSDs, computers, and light dimmers from fixed power loads.

II. BACKGROUND

Instead of fully analyzing the circuit diagram for each new load to compute the estimator, the current waveforms of variable power loads contain information that can be used to distinguish the load from other loads. Current waveforms and discrete Fourier transform (DFT) coefficients of a VSD are shown in Fig. 1. Current waveforms of a computer and a light dimmer are shown in Figs. 2 and 3, respectively. Although,
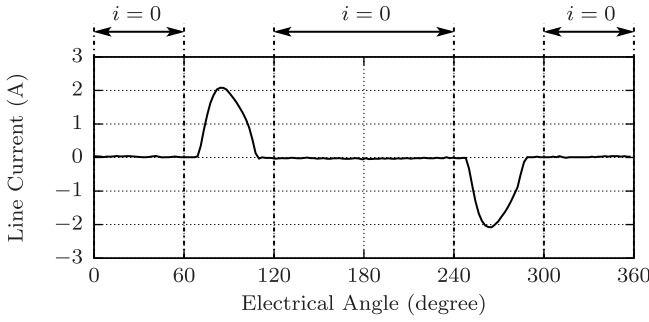
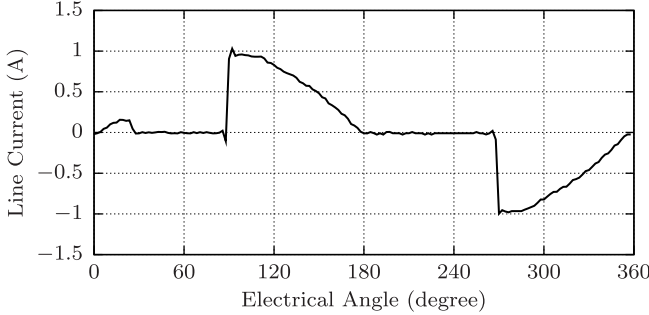Fig. 2. Experimental current waveform of a computer.

Fig. 3. Experimental current waveform of a light dimmer.

the internal circuits of these three loads are different, their current waveforms share a few common properties that can be observed. Those properties include five waveform features:

1) periodicity;
2) presence of zero-current regions;
3) waveform symmetry;
4) approximately band-limited signal;
5) real-valued signal.

These five descriptive constraints can be translated to mathematical forms using the Fourier analysis and synthesis equations.

Given a band-limited and periodic signal, the sampled waveform can be described by a weighted sum of DFT coefficients I_k as

$$i[n] = \sum_{k=0}^{N-1} I_k e^{j\frac{2\pi}{N}(kn)} \tag{1}$$

where the variable n is the time index, ranging from 0 to $N-1$. The number N represents a number of samples per signal period. The DFT coefficients I_k are calculated by the Fourier analysis equation

$$I_k = \frac{1}{N} \sum_{n=0}^{N-1} i[n] e^{-j\frac{2\pi}{N}(kn)} \tag{2}$$

where the subscript k represents the harmonic, ranging from 0 to $N-1$ [20]. The scaling factor $1/N$ normalizes the coefficients by the data length. The relationship in (1) illustrates the form of the functional relationship among different harmonics and the time-domain waveform.

If all N samples of the current waveform are known, the Fourier synthesis equation (1) provides all constraints

between different harmonic currents I_k and the time-domain signal $i[n]$. However, only a limited number of equations can be used to compute the estimator. The next section explains the systematic procedure to translate the five waveform features into the mathematical constraints that can be manipulated into the desired estimator.

III. ESTIMATOR DERIVATION

The goal of the proposed method is to compute a functional relationship between the fundamental harmonic, I_1 and higher harmonics that are uniquely or largely associated with a variable power load at a target site. Specifically, this proposed method is looking for an estimating function in a linear form

$$\widehat{I_1} = \sum_{m=1}^{2K} (c_m I_m) \tag{3}$$

where $\widehat{I_1}$ is the estimated fundamental harmonic, and the coefficient c_m represents a coefficient, which can be complex. The variable I_m represents selected higher harmonics or input harmonics uniquely associated with the variable power load. The number $2K$ represents the number of input harmonics used in the estimator.

The estimator can be developed iteratively with a four-step process.

1) Identify signal constraints.
2) Setup a Fourier matrix equation.
3) Solve for the estimator.
4) Evaluate estimation error.

The first step describes how to translate the five waveform features to linear constraints described in the Fourier synthesis equation (1). This step also includes the selection of the input harmonics used in the estimator. The second step establishes a matrix equation from the constraints. The third step demonstrates how to reduce the matrix equation into the estimator equation. Lastly, the derived estimator is evaluated and tested against accuracy requirements in the fourth step. The procedure can be iterated to further improve the estimation error or to reduce the number of input harmonics.

A. Signal Constraints

First, the current signal is assumed to be periodic with a period of T. In the ac system, the period is a reciprocal of line voltage frequency. The periodic signal is sampled and analyzed using the DFT to obtain the DFT coefficients or current harmonics I_k according to the Fourier analysis equation (2). The signal is assumed to be sampled at the rate F_s such that the sampled signal consists of N points per period. Given N samples per period, there are N DFT coefficients from the Fourier analysis equation (2).

Second, the current waveform consists of known regions of zero-current because of the circuit operation. In the case of a VSD, the consumed current has known zero-current regions shown in Fig. 1, which can be expressed mathematically based on an electrical angle specified in radians

$$i[n] = 0 \quad \text{for} \quad \frac{2\pi n}{N} \in \left[0, \frac{\pi}{6}\right] \cup \left[\frac{5\pi}{6}, \frac{7\pi}{6}\right] \cup \left[\frac{11\pi}{6}, 2\pi\right). \tag{4}$$

For a periodic signal $i[n]$ sampled with the rate of N points per period, the first region of zero-current specified in (4) $0 \leq 2\pi n/N \leq \pi/6$ can be expressed mathematically using the Fourier synthesis equation (1) as

$$
\begin{aligned}
I_0 + I_1 \quad & + \cdots + I_{N-1} & = i[0] \\
I_0 + I_1 e^{j\frac{2\pi}{N}} \quad & + \cdots + I_{N-1} e^{j\frac{2\pi}{N}(N-1)} & = i[1] \\
I_0 + I_1 e^{j\frac{2\pi}{N}(2)} \quad & + \cdots + I_{N-1} e^{j\frac{2\pi}{N}(N-1)(2)} & = i[2] \\
& \vdots & = \vdots \\
I_0 + I_1 e^{j\frac{2\pi}{N}(N_1)} & + \cdots + I_{N-1} e^{j\frac{2\pi}{N}(N-1)(N_1)} & = i[N_1]
\end{aligned} \quad (5)
$$

where $2\pi N_1/N = \pi/6$. Similarly, other zero-current regions can also be translated and added to the list of constraints similar to (5) as well.

Third, the load current waveform exhibits a specific symmetry. Load currents shown in Figs. 1–3 are approximately odd-symmetric. There are two ways to express this constraint. One method is to express in the time domain as

$$
i[n] = -i\left[n + \frac{N}{2}\right], \text{ for } 0 \leq n < \frac{N}{2}. \quad (6)
$$

The number $N/2$ indicates the midpoint of the waveform. Alternatively, the constraint can be formulated in the frequency domain as zero even harmonics, specifically

$$
I_{k_{\text{even}}} = 0 \quad (7)
$$

where the subscript k_{even} represents an even number, including zero. This constraint (7) eliminates all even harmonics from the calculation.

Moreover, a VSD does not consume any triplen harmonic under a balanced three-phase voltage. This constraint can be represented as

$$
I_{k_{\text{triplen}}} = 0. \quad (8)
$$

Fourth, the current signal is processed through the anti-aliasing filter and the analog-to-digital converter in order to be converted into a digital form properly. The anti-aliasing filter confines the bandwidth of the signal, making the signal approximately band-limited. The histogram of DFT coefficients of a VSD in Fig. 1 shows that most energy of the current waveform is contained in a low frequency region. The amplitude of higher harmonics are small and can be neglected. The band-limited constraint can be expressed as

$$
I_{k_{\text{highfreq}}} = 0 \quad (9)
$$

for some $k_{\text{highfreq}} > K_0$, where the parameter K_0 is a user-specified boundary.

Fifth, the real input signal dictates the characteristics of the DFT coefficients, I_k. Given a real signal, the magnitude of the DFT coefficients I_k is even, and the phase the DFT coefficients I_k is odd. In other words, most DFT coefficients are complex conjugate pairs, $I_{N-5} = I_5^*$, for example. The complex conjugate can be used in the selection of the input harmonics.

The estimating function shown in (3) specifies a subset of DFT coefficients as input harmonics. In this paper, the estimator is derived iteratively as a function of input harmonics, the algorithm must be initialized to a reasonable number of harmonics, i.e., ten, with the goal to reduce this number as low as possible. The iterative process will reduce the number of input harmonics when possible.

The selection of the input harmonics depends on two factors. The availability of the harmonics in the measured signals and the estimation error. In the field, the NILM must observe a collection of harmonics that are uniquely associated with the variable load. With the exception of the fundamental harmonic, other harmonics can be selected as input harmonics in the proposed method. The "input" harmonics should at least correlate with the fundamental harmonic and have nonzero values.

Among the available harmonics, the input harmonics with larger magnitude should be selected to minimize the error from noise and to improve the signal-to-noise ratio. One selection scheme is to select the input harmonics according to their magnitudes in a descending order. For example, according to the histogram of the current harmonics shown in Fig. 1, the fifth and seventh harmonics are the two largest harmonics among higher harmonics. Therefore, these two harmonics can be selected as the candidates.

The real input signal implies the complex conjugate property of the DFT coefficients. The magnitude of the complex conjugate pair is the same as the harmonic itself. In the actual implementation, not all DFT coefficients have to be computed in real time. Only the input harmonics are necessary in the estimation. The complex conjugate pair requires no additional computation. As a result, the complex conjugate pairs of the candidate input harmonics can be used as the input harmonics with a negligible computational cost. The number of input harmonic pairs used in the estimator is denoted by the symbol K. In the case of VSD, a possible input harmonic vector for the first iteration can be

$$
I_{\text{input}} = \left[\, I_5, I_5^*, I_7, I_7^*, I_{11}, I_{11}^* \,\right]^T. \quad (10)
$$

In this case, the estimator uses three input harmonic pairs, $K = 3$. The input vector is arranged according to the magnitude size in descending order. After the evaluation process, which is described in the next subsections, the smallest harmonic and its complex conjugate can be removed in the next iteration in order to check whether the estimator with two input harmonic pairs, $K = 2$, provides a good estimation. The iteration process keeps reducing the number of input harmonic pairs until the estimation error just satisfies the accuracy requirement.

In this section, all five waveform constraints have been translated into mathematical equations and the input harmonics have been initially selected according to their magnitudes. The system of equations is constructed by collecting constraints in (5) and (7)–(9). Any linearly dependent constraints must be eliminated. In the next step, the constraint equations must be written in a matrix format that can be manipulated conveniently.

B. Matrix Equation

Once all linearly independent constraints have been identified, the matrix equation can be expressed as

$$
AI_{\text{DFT}} = b = \mathbf{0} \quad (11)
$$

where the matrix A contains complex exponential coefficients. The Fourier series coefficients vector, I_{DFT} contains harmonics I_k. The vector b represents a constant zero vector.

To solve for the estimator, the matrix A is constructed to have the dimension of R rows by $R + 2K$ columns. The number of rows R reflects all usable constraints describing the waveform, while the number of columns $R + 2K$ reflects R constraints and the number of input harmonics $2K$, described in the last section. The I_{DFT} can be partitioned into sub-blocks

$$I_{\mathrm{DFT}} = \begin{bmatrix} I_{\mathrm{goal}} & | & I_{\mathrm{others}} & | & I_{\mathrm{input}} \end{bmatrix}^T \qquad (12)$$

where the variable I_{goal} is the estimated harmonic, specifically, the fundamental harmonic, I_1. The vector I_{input} consists of the input harmonic pairs as shown in (10). The vector I_{others} is comprised of other nonzero harmonics. The columns of matrix A have to be rearranged in the similar order

$$A = \begin{bmatrix} A_{\mathrm{goal}} & | & A_{\mathrm{others}} & | & A_{\mathrm{input}} \end{bmatrix} \qquad (13)$$

where the matrix A_{goal} is a column vector of size R-by-1, containing coefficients associated with the goal harmonic, specifically, the fundamental harmonic I_1 in this case. The matrix A_{input} contains all coefficients corresponding to the input harmonics in I_{input} and has a dimension of R-by-$2K$.

After the matrix A and the DFT coefficient vector I_{DFT} have been rearranged in a desired format, the next section shows the manipulation of the matrix A to obtain the estimator. Specifically, the manipulation will modify the matrix A such that it contains a row relating I_{goal}, i.e., I_1, to a small subset of input harmonics I_{input} with all other harmonics in this row having zero coefficients.

C. Reduced Row Echelon Form

Once the system of equations has been set up in the matrix format, the next step is to compute the functional relationship between different harmonics. The algorithm uses a Gaussian elimination method to reduce the matrix A into a reduced row echelon form (RREF), A_{RREF}. After the Gaussian elimination process has been performed, the matrix equation in (11) can be expressed in block matrices as

$$A_{\mathrm{RREF}} I_{\mathrm{DFT}} = \begin{bmatrix} 1 & 0 & C_{\mathrm{goal}} \\ 0 & I & C_{\mathrm{others}} \end{bmatrix} \begin{bmatrix} I_{\mathrm{goal}} \\ I_{\mathrm{others}} \\ I_{\mathrm{input}} \end{bmatrix} = \mathbf{0}. \qquad (14)$$

By rearranging the terms in (14), the estimator can be written as

$$I_{\mathrm{goal}} = -C_{\mathrm{goal}} I_{\mathrm{input}}. \qquad (15)$$

Equation (15) describes a linear estimator for the desired harmonic, I_{goal}, with complex coefficients (11). The estimator computes I_{goal} from observations of input harmonics I_{input}.

This section has demonstrated the manipulation of the matrix equation (11) to obtain the estimator for the fundamental harmonic from the selected input harmonics in I_{input}. This candidate estimator can now be checked to ensure that it can compute the fundamental harmonic associated with a variable load with acceptably small error.

D. Estimator Evaluation

After the estimator has been computed, the estimator is evaluated by performing the estimation of the fundamental harmonic using the actual test current. The performance is measured by the estimation error, which is defined as

$$\text{estimation error}\,(\%) = \left| I_1 - \widehat{I}_1 \right| / |I_1| \times 100 \qquad (16)$$

where the variable I_1 is the measured fundamental harmonic, and the variable $\widehat{I}_1$ is the estimated fundamental harmonic computed by the estimator.

Because the estimator in (15) is computed for a specific number of samples N and a specific set of input harmonics, I_{input}, the estimator may not work well for other sampling rates. The band-limited signal sampled at the sampling frequency above the Nyquist rate should contain all information within the data. If the estimator predicts the fundamental harmonic accurately for a given sampling rate, the estimators derived for higher sampling rates should predict accurately as well because more constraints can be listed in the system of linear equations. The band-limited property should be more accurate as the sampling frequency become higher. The zero harmonics approximation in (9) should also be more accurate. The estimator should accurately predict the fundamental current harmonic over a range of N_{samp} samples per cycle. Fig. 4 shows examples of the estimator evaluation for the VSD.

In this example, the test current is shown in Fig. 1. In the first iteration, the estimators were derived using three harmonic pairs $K = 3$ as listed in (10) and different sample numbers N_{samp}. The estimation errors for $K = 3$ cases are shown in Fig. 4(a). The errors are below 0.4 percent, indicating that the fundamental harmonic of the VSD can be estimated accurately using three harmonic pairs $K = 3$ indicated in (10).

In the next iteration, the input harmonics are reduced to two harmonic pairs the fifth, seventh, and their complex conjugates, $K = 2$. The procedures are reiterated to obtain the estimator for $K = 2$ and different sample points N_{samp}. The estimation errors are shown in Fig. 4(b). The errors are below 2.5 percent across a wide range of sample points N_{samp}. As a result, the VSD estimator can use only two harmonic pairs $K = 2$ to estimate the fundamental harmonic with a reasonable error.

To examine if the number of input harmonics I_{input} can be further reduced, the final iteration was done with $K = 1$, using only the fifth harmonic and its complex conjugate. The estimation errors are shown as a function of sample points N_{samp} in Fig. 4(c). The result demonstrates the estimation error above 10% for many sample points. This result implies that the estimators will not perform consistently across different sample rates. Therefore, the VSD estimator derived using the proposed procedures should use at least two harmonic pairs $K = 2$ to accurately predict the fundamental harmonic.

This section has demonstrated the iterative procedures to derive the estimators based on the five waveform features by using the VSD load as an example. The input harmonics I_{input} are chosen according to their availability and magnitude. The estimator is computed using a simple Gaussian

(a)   (b)

Fig. 5. Vectorial representations of the complex exponential ζ_N^k and the primitive roots of unity for $N = 12$. (a) Possible vectors ζ_N^k. (b) Primitive roots of unity.
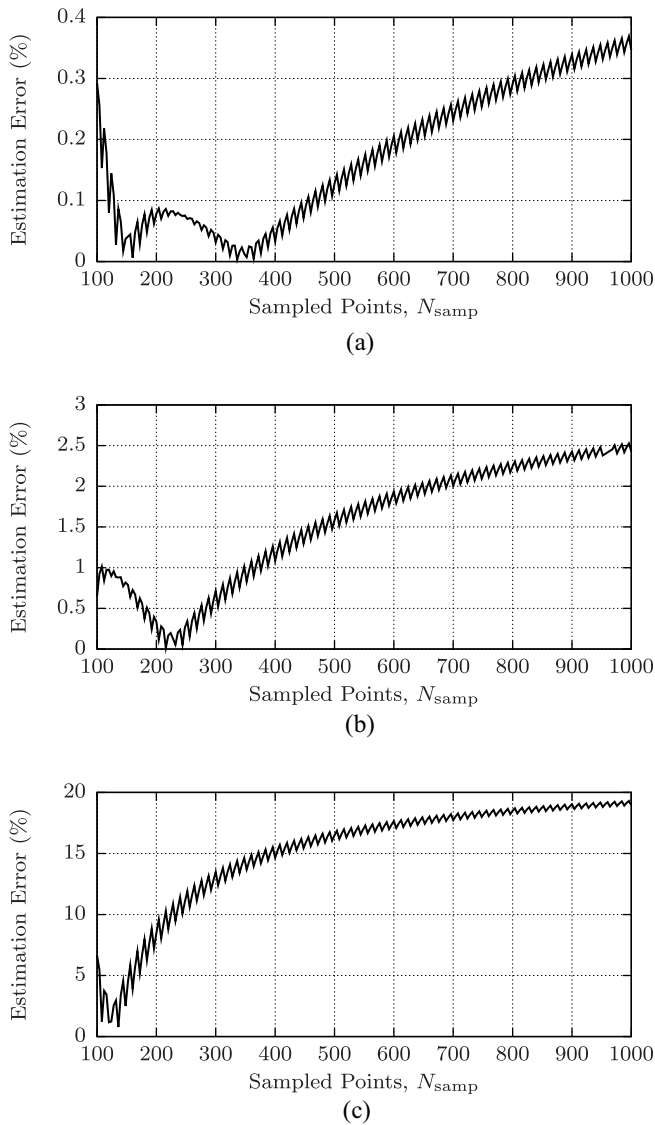

Fig. 4. Example of estimation errors as a function of sample points N_{samp} and input harmonic pairs K. Simulated VSD current waveform was used in these three cases. (a) $K = 3$. (b) $K = 2$. (c) $K = 1$.

elimination algorithm. Then the performance of the estimator is tested for consistency by measuring the estimation error against the test current. The procedures are repeated with the reduced number of input harmonics by removing the harmonic with the smallest magnitude. The iteration is finished when the estimation error exceeds the requirement. The proposed method provides a guideline to compute the estimator in a linear form. A user has the freedom to select the input harmonics for I_{input}. The evaluation process will verify whether an accurate estimator can be derived using the selected harmonics.

Because the estimator is computed for different sample points N_{samp}, the computational error from the floating point arithmetic can mask the potential of the algorithm as the number of sample points N_{samp} increases. To avoid the floating-point error problem, the next section briefly explain the cyclotomic field representation used in the computation of the estimator coefficients.
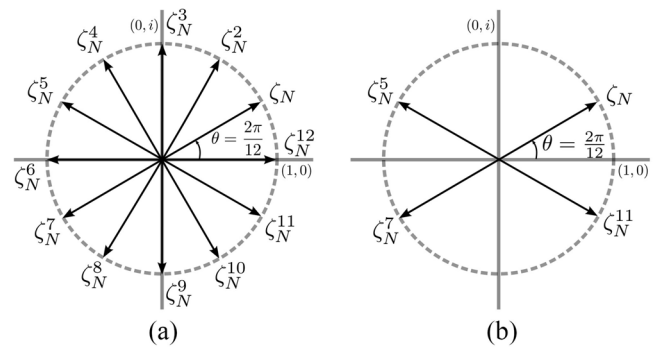
IV. CYCLOTOMIC FIELD REPRESENTATION

Initial tests of the proposed algorithm has shown that the estimation error is largely influenced by the numerical error of the floating point arithmetic used during the row operation. The solution is to convert the representation of coefficients to elements of a cyclotomic field, which allows the RREF algorithm to be calculated more accurately [17]. This section summarizes the cyclotomic field representation and some properties described in [16]–[19].

Recall that the coefficients in the matrix A in (11) are in the forms of $c_k e^{j(2\pi k/N)}$ for an integer $k \in [0, N-1]$ and a rational number c_k and the number N is the number of samples per cycle. The Gaussian elimination method involves only standard arithmetic operations: 1) addition; 2) subtraction; 3) multiplication; and 4) division. After each row operation, each coefficient of the matrix A can be expressed by a polynomial, $p(\zeta_N)$, as

$$p(\zeta_N) = \sum_{k=0}^{N-1} c_k \zeta_N^k \qquad (17)$$

where the variable ζ_N is the complex exponential $e^{j(2\pi/N)}$. The complex exponential has a cyclic property

$$\zeta_N^{(k+N)} = \zeta_N^k. \qquad (18)$$

The exponent power is always a modulo-N integer. As a result, the polynomial would never grow more than N terms with the highest power being $N-1$, specifically $e^{j(2\pi(N-1)/N)}$. Furthermore, the complex exponential $e^{2\pi/N}$ is a primitive root of unity, which can be used a basis to generate others complex exponentials in the polynomial $p(\zeta_N)$. Possible complex exponentials and four possible primitive roots of unity in the case of $N = 12$ are shown in Fig. 5. Because the complex exponentials belong to a finite set, it is advantageous to handle them symbolically in computation. In fact, all elements of the matrix A belong to a cyclotomic field $\mathbb{Q}[\zeta_N]$, where the symbol $\mathbb{Q}$ represents a set of rational numbers and the symbol $\mathbb{Q}[\zeta_N]$ is also a field created by adjoining the primitive root ζ_N to the rational numbers $\mathbb{Q}$ [17].

The most important property of a field for the proposed estimator is that a field is closed under arithmetic operations: 1) addition; 2) subtraction; 3) multiplication; and 4) division.
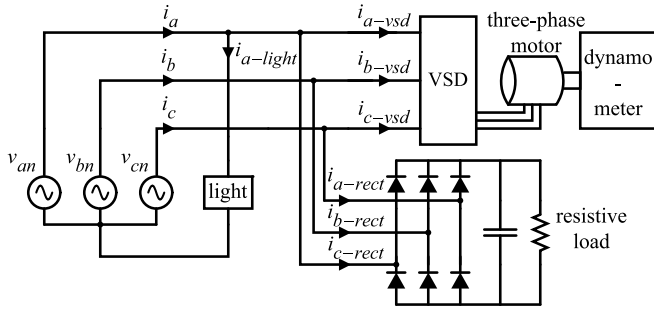
Fig. 6. Experimental setup for extracting the VSD and three-phase rectifier power from the incandescent light bulb.

This property implies that an arithmetic operation between two elements in the field results in the element of the field. As a result, the Gaussian elimination can be computed exactly with the cyclotomic field representation. One method is to store only the rational numbers c_k of the polynomial $p(\zeta_N)$ in (17) throughout the entire operation. After the Gaussian elimination process is finished, the value of the coefficient can be obtained by substituting the floating point representation of ζ_N in the final polynomial. This substitution is the only step that the rounding error occurs in the entire computation.

In addition, the right hand side of the system of the (11) is a zero vector. In this case, the operation can be done using only integer values because the denominator can be normalized without affecting the accuracy. In this paper, all calculations are done using rational numbers. The computation is implemented in the GP-Pari mathematical language, which provides necessary operations for manipulating elements of the cyclotomic field [21].

V. EXPERIMENTAL RESULTS AND DISCUSSION

This section demonstrates the ability of the estimator to extract variable power loads such as VSDs, computers, and light dimmers from a fixed linear load. All input signals used in these experiments were sampled at the rate of 8 kHz.

The first test involves extracting a VSD and three-phase rectifier power from a 50-W incandescent light bulb. The experimental setup is shown in Fig. 6. The estimated fundamental harmonic current of the VSD is given by

$$\widehat{I}_1^{\text{vsd}} = (1.358 - 0.102j) I_5 + (-0.903 - 0.102j) I_5^*$$
$$+ (0.731 - 0.082j) I_7 + (-0.547 - 0.082j) I_7^*. \quad (19)$$

The estimated current is computed independently for each phase.

The fundamental real and reactive powers of the three-phase load are computed by

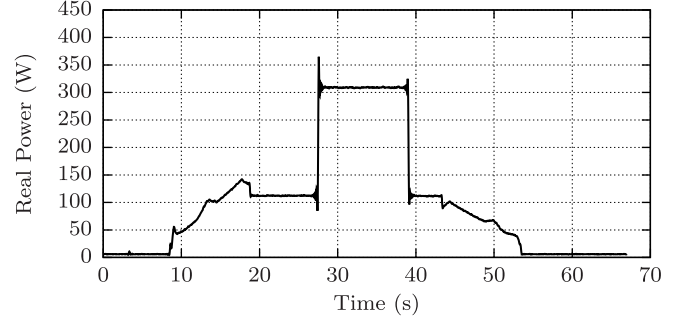$$P_{3-\text{ph}} = \frac{1}{2}\mathcal{R}\text{e}\left(V_{a1}I_{a1}^* + V_{b1}I_{b1}^* + V_{c1}I_{c1}^*\right) \quad (20)$$

and

$$Q_{3-\text{ph}} = \frac{1}{2}\mathcal{I}\text{m}\left(V_{a1}I_{a1}^* + V_{b1}I_{b1}^* + V_{c1}I_{c1}^*\right) \quad (21)$$
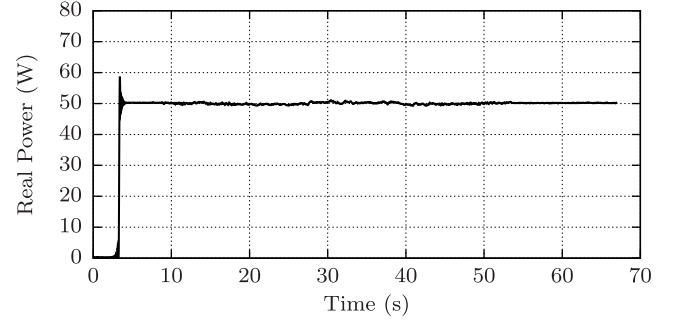
respectively. The line-to-neutral voltages are measured in this experiment and only the fundamental harmonic components are used in the power calculation.
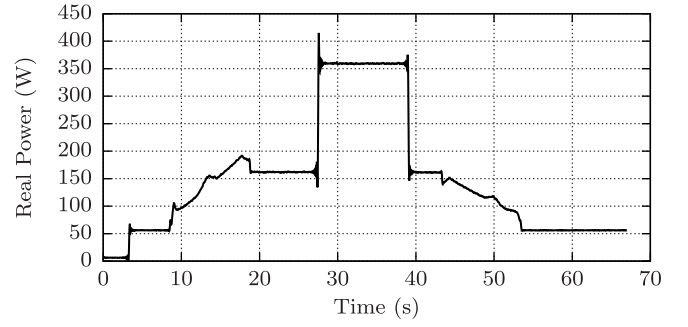
Fig. 7. Demonstration of the waveform-based estimator extracting the VSD and three-phase rectifier power consumption from an incandescent light. The light bulb turns on at the time $t = 4$ s and never turns off. The VSD starts up at the time $t = 8$ s and reaches the steady state at the time $t = 18$ s. The fixed-load, three-phase rectifier then turns on at the time $t = 27$ s and turns off at the time $t = 39$ s. The VSD starts to ramp down the power at the time $t = 43$ s and completely stops at the time $t = 53$ s. (a) Total real power of the VSD, three-phase rectifier, and the incandescent light. Estimated real power consumed by the (b) VSD and three-phase rectifier and (c) incandescent light.

The fundamental real and reactive powers of the single phase load are defined as

$$P_{1-\text{ph}} = \frac{1}{2}\mathcal{R}\text{e}\left(V_1 I_1^*\right) \text{ and } Q_{1-\text{ph}} = \frac{1}{2}\mathcal{I}\text{m}\left(V_1 I_1^*\right) \quad (22)$$

respectively.

Fig. 7 depicts the extraction of real power of the VSD and a three-phase rectifier load from a 50-W incandescent light. The extraction result resembles the operation of the VSD and the three-phase rectifier. The residual power clearly shows a constant power consumption of the incandescent light.

In the case of a computer, the estimator is derived using the zero-current regions shown in Fig. 2. The computer is
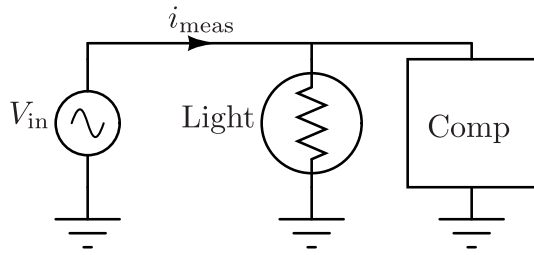
Fig. 8.   Experimental setup for resolving the power consumption of the computer from the incandescent light bulb.

expected to consume the current during the window specified as a function of electrical angle specified in radians

$$i[n] = 0 \text{ for } \frac{2\pi n}{N} \in \left[0, \frac{\pi}{3}\right] \cup \left[\frac{2\pi}{3}, \frac{4\pi}{3}\right] \cup \left[\frac{5\pi}{3}, 2\pi\right). \quad (23)$$

The computer estimator is given by

$$\begin{aligned}
\widehat{I}_1^{\text{comp}} = &(-0.744 - 1.214j)\, I_3 + (-0.324 - 0.636j)\, I_3^* \\
&+ (0.458 - 0.898j)\, I_5 + (-0.673 - 0.530j)\, I_5^* \\
&+ (0.326 - 0.026j)\, I_7 + (-0.145 + 0.200j)\, I_7^*. \quad (24)
\end{aligned}$$

The experimental setup and experimental results are shown in Figs. 8 and 9, respectively. Experimental results show that the power consumption of the computer can be cleanly extracted from the aggregate measurements. The residual power consumption clearly shows the operations of the incandescent light bulb with a constant power consumption.

In the last experiment, the coefficients of the estimator are computed in order to extract the power consumption of the TRIAC-based light dimmer. The dimmer adjusts the brightness and power consumption by varying the firing angle of the TRIAC to chop off the sinusoidal input voltage feeding the incandescent light bulb as shown in Fig. 3 for example. The estimator for the light dimmer has been developed similar to (24). The estimator uses an approximated current waveform without the initial current at the beginning of the cycle. This approximation allows the five waveform events to be easily distinguished. In the case of a light dimmer, four harmonic pairs are used to estimate the fundamental harmonic currents. Specifically, the estimator uses the third, fifth, seventh, and ninth harmonics. The detail of the estimator for the light dimmer are described in [22].

The test setup for the light dimmer experiment is shown in Fig. 10. Experimental results are shown in Figs. 11 and 12. Experimental results demonstrate that the estimator can track the real and reactive power consumption of the light dimmer accurately. The extracted power consumption of the light dimmer in Fig. 11(b) clearly resembles the operation of the light dimmer. The residual power shown in Fig. 11(c) shows a constant real power of 250-W consumed by the incandescent light as expected. Furthermore, almost all of the reactive power is consumed by the light dimmer. The estimator tracks the reactive power accurately as shown in Fig. 12.
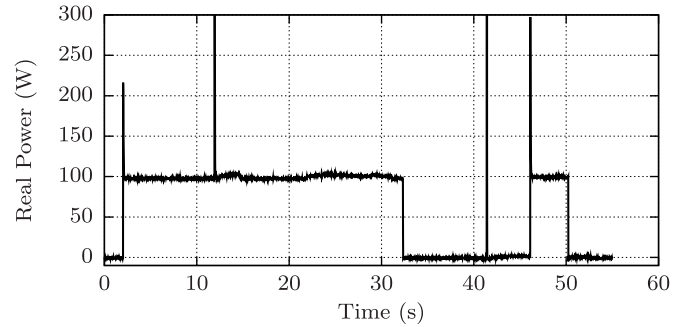
Three experimental results demonstrate the ability of the waveform-based estimator to resolve and track the power consumption of variable power loads accurately. The estimator is derived using the four-step process that computes the estimator
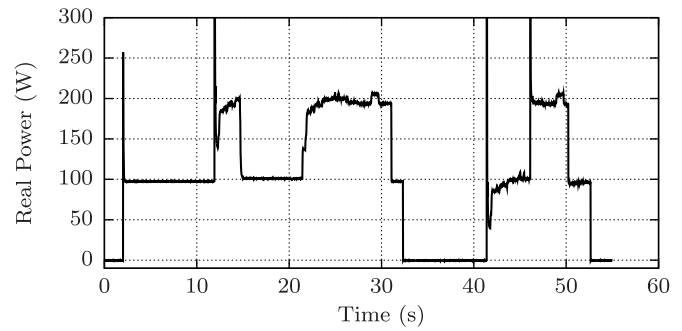
(a)
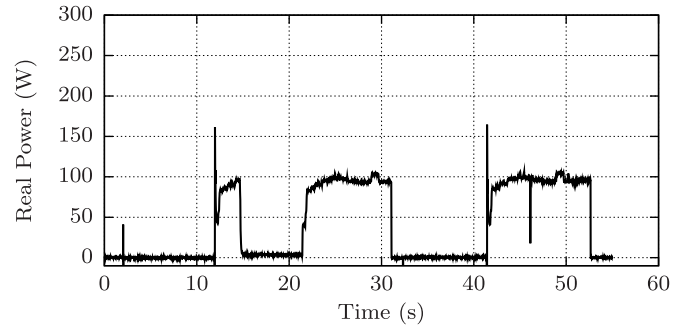
(b)

(c)

Fig. 9.   Demonstration of the waveform-based estimator extracting a computer's power consumption from an incandescent light. The light turns on at $t = 2$ s and turns off at $t = 32$ s. The computer was turned on at $t = 12$ s and turned off at $t = 15$ s. The computer was turned on again at $t = 22$ s and turned off at $t = 31$ s. Finally, the computer was turned on at $t = 42$ s and turned off at $t = 53$ s. During the last computer activity, the light was turned on at $t = 46$ s and turned off at $t = 50$ s. (a) Aggregate real-power consumption of the computer and the incandescent light. Estimated real power consumed by the (b) computer and (c) incandescent light.
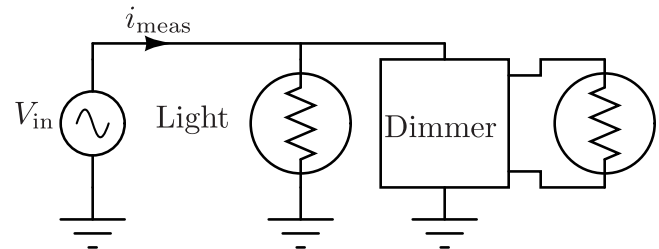

Fig. 10.   Experimental setup for resolving the power consumption of the TRIAC-based light dimmer from the incandescent light bulb.

for a variable power load using only the five waveform features in the measured currents. The iterative process systematically reduces the number of input harmonics used for estimation
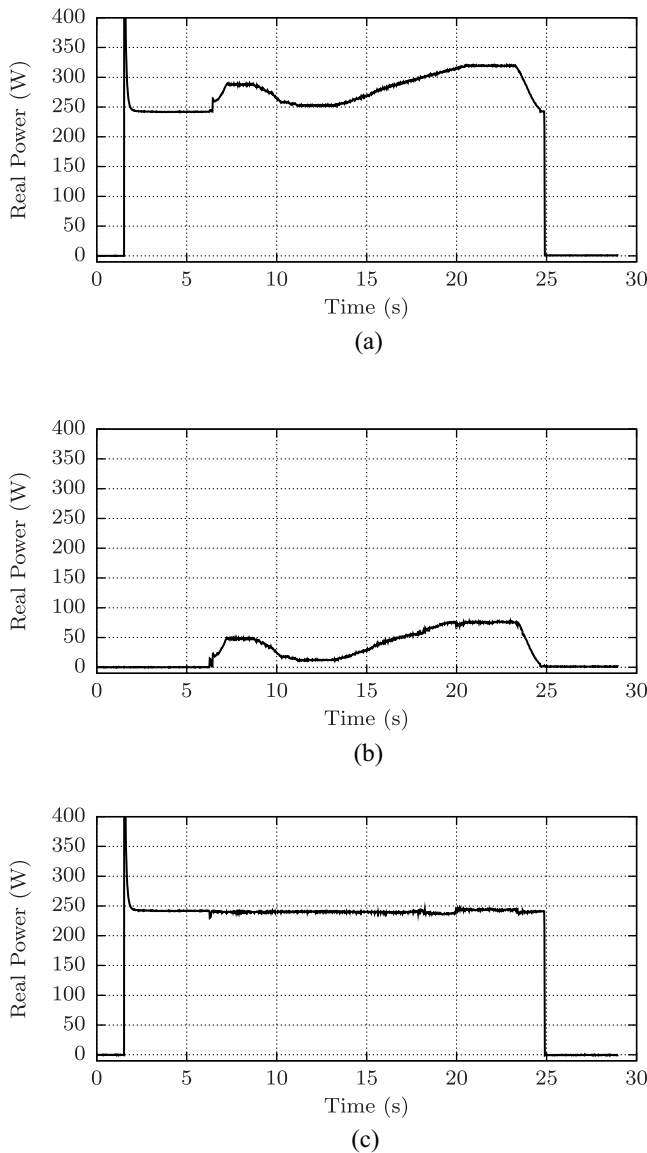
(a)

(b)

(c)

Fig. 11. Demonstration of the waveform-based estimator extracting a light dimmer's power consumption from an incandescent light. (a) Real-power consumption of both the incandescent light and the light dimmer. The 250-W light was turned on at $t = 2$ s. Next, the light dimmer was turned on at $t = 7$ s. The power consumption of the dimmer was varied continuously. Finally, both the incandescent light and the light dimmer were turned off at $t = 25$ s. Estimated real power consumed by the (b) light dimmer and (c) incandescent light bulb.

to the smallest number. The estimator is computed offline by determining the coefficients for different input harmonics. Use of the estimator in a real-time monitoring environment only involves a few multiplication and addition operations.

VI. CONCLUSION

This paper has demonstrated a waveform-based estimator able to extract the power consumption of variable power loads from fixed power loads. The proposed method provides a systematic process to derive an estimator for any variable power load with structural features in the current waveforms without a full analysis of internal circuits. The method can possibly be applied for other variable power loads with unique waveform
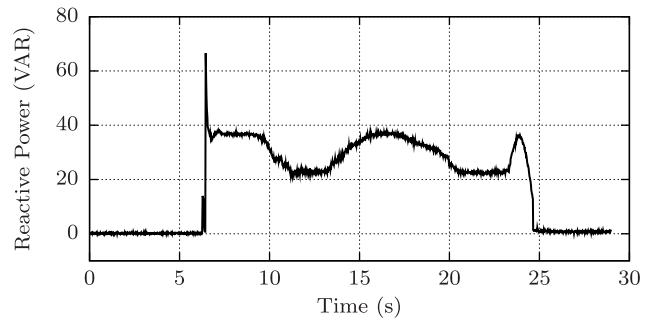

Fig. 12. Demonstration the waveform-based estimator tracking the reactive power consumed by the light dimmer. The reactive power is mostly consumed by the light dimmer.

features. The ability to disaggregate the power consumption of each load could supplement the smart metering device in the area of diagnostic monitoring, where potential health issues of electrical loads can be monitored and detected in an early stage. The early warning can potentially save a major repair cost and minimize the operational downtime. Additionally, the information of the power consumption of each load can be used in scheduling the load and optimizing the operation of electrical loads in the system. The proposed algorithm uses a centralized monitoring system where only a single set of voltage and current sensors can monitor a group of loads together, saving the cost of additional sensors at each load.

REFERENCES

[1] K. D. Lee *et al.*, "Estimation of variable-speed-drive power consumption from harmonic content," *IEEE Trans. Energy Convers.*, vol. 20, no. 3, pp. 566–574, Sep. 2005.
[2] P. Ducange, F. Marcelloni, and M. Antonelli, "A novel approach based on finite-state machines with fuzzy transitions for nonintrusive home appliance monitoring," *IEEE Trans. Ind. Informat.*, vol. 10, no. 2, pp. 1185–1197, May 2014.
[3] E. Proper *et al.*, "Field demonstration of a real-time non-intrusive monitoring system for condition-based maintenance," in *Proc. Elect. Ship Design Symp.*, National Harbor, MD, USA, Feb. 2009, pp. 1–8.
[4] U.S. Department of Energy, "The smart grid: An introduction," Tech. Rep., 2008.
[5] S. B. Leeb, S. R. Shaw, and J. L. Kirtley, "Transient event detection in spectral envelope estimates for nonintrusive load monitoring," *IEEE Trans. Power Del.*, vol. 10, no. 3, pp. 1200–1210, Jul. 1995.
[6] S. R. Shaw, S. B. Leeb, L. K. Norford, and R. W. Cox, "Nonintrusive load monitoring and diagnostics in power systems," *IEEE Trans. Instrum. Meas.*, vol. 57, no. 7, pp. 1445–1454, Jul. 2008.
[7] C. R. Laughman *et al.*, "Power signature analysis," *IEEE Power Energy Mag.*, vol. 1, no. 2, pp. 56–63, Mar. 2003.
[8] S. R. Shaw and C. Laughman, "A Kalman-filter spectral envelope preprocessor," *IEEE Trans. Instrum. Meas.*, vol. 56, no. 5, pp. 2010–2017, Oct. 2007.
[9] J. Paris *et al.*, "Scalability of non-intrusive load monitoring for shipboard applications," in *Proc. Amer. Soc. Naval Engineers Day*, National Harbor, MD, USA, Apr. 2009, pp. 1–9.
[10] M. Dong, P. Meira, W. Xu, and W. Freitas, "An event window based load monitoring technique for smart meters," *IEEE Trans. Smart Grid*, vol. 3, no. 2, pp. 787–796, Jun. 2012.
[11] D. Srinivasan, W. S. Ng, and A. Liew, "Neural-network-based signature recognition for harmonic source identification," *IEEE Trans. Power Del.*, vol. 21, no. 1, pp. 398–405, Jan. 2006.
[12] W. Chan, A. T. P. So, and L. L. Lai, "Wavelet feature vectors for neural network based harmonics load recognition," in *Proc. Int. Conf. Adv. Power Syst. Control Oper. Manage. (APSCOM)*, vol. 2. Oct. 2000, pp. 511–516.

[13] M. Dong, P. Meira, W. Xu, and W. Freitas, "An event window based load monitoring technique for smart meters," *IEEE Trans. Smart Grid*, vol. 3, no. 2, pp. 787–796, Jun. 2012.

[14] M. Dong, P. Meira, W. Xu, and C. Chung, "Non-intrusive signature extraction for major residential loads," *IEEE Trans. Smart Grid*, vol. 4, no. 3, pp. 1421–1430, Sep. 2013.

[15] W. Wichakool, A. Avestruz, R. W. Cox, and S. B. Leeb, "Modeling and estimating current harmonics of variable electronic loads," *IEEE Trans. Power Electron.*, vol. 24, no. 12, pp. 2803–2811, Dec. 2009.

[16] L. C. Washington, *Introduction to Cyclotomic Fields*, 2nd ed. New York, NY, USA: Springer, 1997.

[17] Z. Remscrim, "The theory and application of non-intrusive load monitoring," Master's thesis, Dept. Elect. Eng. Comput. Sci., Mass. Inst. Technol., Cambridge, MA, USA, 2010.

[18] J. H. W. Lenstra, "Euclid's algorithm in cyclotomic fields," *J. London Math. Soc.*, vol. 2, no. 10, pp. 457–465, 1975.

[19] J. M. Masley and H. L. Montgomery, "Cyclotomic fields with unique factorization," *J. Reine Angew. Math.*, vol. 1976, nos. 286–287, pp. 248–256, 1976.

[20] A. V. Oppenheim, R. W. Schafer, and J. R. Buck, *Discrete-time Signal Processing*, 2nd ed. Upper Saddle River, NJ, USA: Prentice-Hall, 1999.

[21] K. Belabas. (2010). *PARI/GP development headquarters* [Online]. Available: http://pari.math.u-bordeaux.fr/

[22] W. Wichakool, "Advanced nonintrusive load monitoring system," Ph.D. thesis, Dept. Elect. Eng. Comput. Sci., Massachusetts Inst. Technol., Cambridge, MA, USA, Feb. 2011.

Zachary Remscrim is currently a Graduate Student with the Massachusetts Institute of Technology, Cambridge, MA, USA.

Uzoma A. Orji received the Ph.D. degree in electrical engineering and computer science from the Massachusetts Institute of Technology, Cambridge, MA, USA, in 2013.

Warit Wichakool (S'05–M'09) received the Ph.D. degree in electrical engineering and computer science from the Massachusetts Institute of Technology, Cambridge, MA, USA, in 2011.

His current research interests include power conversion, instrumentation, system modeling, analog circuit design, and signal processing for power electronics applications.

Steven B. Leeb (F'87) received the Doctoral degree in electrical engineering and computer science from the Massachusetts Institute of Technology (MIT), Cambridge, MA, USA, in 1993.

He has been a member of the faculty of the Department of Electrical Engineering and Computer Science, MIT, since 1993, and holds a joint appointment in the Department of Mechanical Engineering. His research interests include the development of signal processing algorithms for energy and real-time control applications.